

GEOMETRY OF THE VISUAL CORTEX WITH APPLICATIONS TO IMAGE INPAINTING AND ENHANCEMENT

FRANCESCO BALLERIN AND ERLEND GRONG

ABSTRACT. Equipping the rototranslation group $SE(2)$ with a sub-Riemannian structure inspired by the visual cortex V1, we propose algorithms for image inpainting and enhancement based on hypoelliptic diffusion. We innovate on previous implementations of the methods by Citti, Sarti, and Boscain et al., by proposing an alternative that prevents fading and is capable of producing sharper results in a procedure that we call **WaxOn-WaxOff**. We also exploit the sub-Riemannian structure to define a completely new unsharp filter using $SE(2)$, analogous to the classical unsharp filter for 2D image processing. We demonstrate our method on blood vessels enhancement in retinal scans.

1. INTRODUCTION

Image inpainting is a process that aims at restoring information that has been lost in a region of the canvas. Although in recent times neural networks have proven to be extremely effective at most digital image processing tasks, the black box structure of most implementations makes such tools difficult to understand and trust, as well as prone to unexpected failures. Moreover, the computational requirements to train such networks can often be prohibitive.

The aim of this work is to introduce a new lightweight, robust, and effective algorithm for image inpainting and image enhancement based on a well-known sub-Riemannian model of the visual cortex V1.

This geometric structure was formalized by Petitot in 1998 [32, 33] and exploited by Citti and Sarti [15, 16] and Boscain et al. [7, 9, 10, 11, 12, 13] to derive a biologically inspired image restoration algorithm. The algorithm is blind, i.e. it does not exploit information on the position of the corruption. The main idea of this approach is that by lifting the image from \mathbb{R}^2 to $SE(2)$ restoration can be achieved by hypoelliptic diffusion in the direction of the lifted level curves of the image.

The main drawback of this family of algorithms is that, by design, the resulting images incur heavy blurring and loss of higher-frequency information. We aim at tackling such problems by exploiting the sub-Riemannian structure on $SE(2)$, and the vector field that is transversal to the lifted level lines of the image, to produce sharpening tools. By alternating diffusion along level curves (**WaxOn**) with concentration transversally to the level curves and in the direction of the gradient (**WaxOff**), we are able to produce inpainting in the damaged areas while also preserving sharpness.

In addition to image inpainting, transversal diffusion allows us to design a completely new sharpening filter, analogous to the classic 2D unsharp filter, with applications to image enhancement and preprocessing. We demonstrate our new method by enhancing blood vessels in a retinal

2020 *Mathematics Subject Classification.* Primary 94A08; Secondary 35H10, 53C17, 93C20.

Key words and phrases. image inpainting, image enhancement, neurogeometry, sub-Riemannian diffusion, rototranslation group, unsharp filter, level curve completion.

The authors are supported by the grant GeoProCo from the Trond Mohn Foundation - Grant TMS2021STG02 (GeoProCo). Part of the results of this paper has appeared in the first author's master thesis.

scan. By combining this unsharp filter with the a new procedure that we call `WaxOff`, we also propose an inpainting method that preserves even more high-frequency details, and allows for longer diffusion times without excessive blurring.

Section 2 briefly introduces the geometrical preliminaries needed to understand the sub-Riemannian model of the visual cortex V1. For more details on sub-Riemannian geometry, we refer to Appendix A. In section 3 we present the previous work by Citti and Sarti [16] and Boscain et al. [11] on exploiting the sub-Riemannian geometry of the V1 model for image restoration. In section 4 we present our new developments on the subject, which consist of a new approach to treat images in the geometrical model of interest and two approaches based on sharpening techniques to address blurring, one being the `WaxOff`-procedure and the other the unsharp filter on $SE(2)$. We also present a Python package that has been developed in conjunction with this article, from which all figures of this work are derived.¹

We thank Xavier Pennec for the helpful discussions around the `WaxOff` procedure and Francesco Rossi for sharing with us a MATLAB implementation of the algorithm, which was an inspiration for our own implementation.

Related work. Extensive work has been presented in the study of the Lie Group $SE(2)$ relative to image processing, with special attention to the field of retinal imagery. We give in this section an overview of related works.

Citti and Sarti [15, 16] have presented a framework based on mean curvature flow to achieve restoration through diffusion by performing perception completion in the space $SE(2)$ followed by non-maxima suppression in the same space. Work by Franken and Duits has been done to study the possible ways to enhance and sharpen the effects of the proposed algorithms [17, 19]. Boscain et al. have expanded on these methods [11] and have deepened the discussion by proposing a semidiscrete treatment of the problem as well as a variation of the problem in which the position of the corruption is known [9, 10, 13]. Other works have focused on the specific application of retinal vessel analysis exploiting the geometric structure of $SE(2)$ as orientation scores, for example in [5, 22, 41]. In addition the Lie Group $SE(2)$ has been successfully used in the context of geometric deep learning [6], introducing an $SE(2)$ group convolution layer that allows for a state-of-the-art performance without the need for data augmentation in problems within histopathology, retinal imaging, and electron microscopy.

2. SUB-RIEMANNIAN GEOMETRY AND IMAGE PROCESSING

2.1. Geometry of the rototranslation group. We consider *the special euclidean group* $SE(2)$ of dimension 2, as the group of matrices

$$(2.1) \quad SE(2) = \left\{ B = \begin{bmatrix} A & \mathbf{x} \\ 0 & 1 \end{bmatrix} \mid \begin{array}{l} \mathbf{x} \in \mathbb{R}^2, \\ A \in SO(2) \end{array} \right\} = \left\{ \begin{bmatrix} \cos \theta & -\sin \theta & x \\ \sin \theta & \cos \theta & y \\ 0 & 0 & 1 \end{bmatrix} \mid \begin{array}{l} x, y \in \mathbb{R}, \\ \theta \in \mathbb{R}/2\pi\mathbb{Z} \end{array} \right\}$$

which is a matrix Lie group, i.e. both a group under matrix multiplication and a smooth manifold. $SE(2)$ is the group of all transformations on \mathbb{R}^2 which preserve distances, orientations, and angles (rigid transformations). Any such transformation can be written as a rototranslation

$$\begin{aligned} T : \mathbb{R}^2 &\rightarrow \mathbb{R}^2 & A &\in SO(2) \\ \mathbf{a} &\mapsto A\mathbf{a} + \mathbf{x} & \mathbf{x}, \mathbf{a} &\in \mathbb{R}^2. \end{aligned}$$

Using the coordinates (x, y, θ) in (2.1), we see that $SE(2)$ as a space can be identified with the 3-dimensional cylinder $\mathbb{R}^2 \times S^1$.

¹Package can be found at <https://github.com/ballerin/v1diffusion>.

A vector field X on $SE(2)$ is called *left invariant* if it has the property that any curve $\gamma(t)$ is tangent to X if and only if $B\gamma(t)$ is tangent to X for any $B \in SE(2)$. Any such vector field will be a linear combination of vector fields X_1 , X_2 and X_3 , written in the coordinates (x, y, θ) as

$$(2.2) \quad X_1 = \cos(\theta)\partial_x + \sin(\theta)\partial_y, \quad X_2 = \partial_\theta, \quad X_3 = -\sin(\theta)\partial_x + \cos(\theta)\partial_y.$$

These vector fields have flows $e^{tC_j}(B) = B \exp(tC_j)$, where

$$C_1 = \begin{bmatrix} 0 & 0 & 1 \\ 0 & 0 & 0 \\ 0 & 0 & 0 \end{bmatrix}, \quad C_2 = \begin{bmatrix} 0 & -1 & 0 \\ 1 & 0 & 0 \\ 0 & 0 & 0 \end{bmatrix}, \quad C_3 = \begin{bmatrix} 0 & 0 & 0 \\ 0 & 0 & 1 \\ 0 & 0 & 0 \end{bmatrix}.$$

Here we have used e^{tX} for the flow of the vector field X , while $\exp(C) = \sum_{j=0}^{\infty} \frac{C^j}{j!}$ denotes the usual exponential of matrix C .

Recall that *Lie bracket of vector fields* X and Y is the vector field $[X, Y]$ defined by $[X, Y]f = X(Yf) - Y(Xf)$. We note that the Lie bracket of left-invariant vector fields is always left-invariant, and for the basis in (2.2), we obtain

$$[X_1, X_2] = -X_3, \quad [X_2, X_3] = X_1, \quad [X_1, X_3] = 0.$$

We observe in particular that we can obtain X_3 by combining X_1 and X_2 . We will take advantage of this in what follows. By letting $\mathcal{H} = \text{span}\{X_1, X_2\}$ we obtain a bracket-generating distribution, which guarantees under Chow-Rashevskii's theorem that any two points in $SE(2)$ can be connected by a path whose tangent vectors lie in the distribution \mathcal{H} . See Appendix A.1 for details. Similarly, if we consider a horizontal distribution $\tilde{\mathcal{H}} = \text{span}\{X_2, X_3\}$, then we can obtain X_1 as the bracket $[X_2, X_3] = X_1$ so that this distribution is also bracket-generating. We will use both for our proposed algorithm.

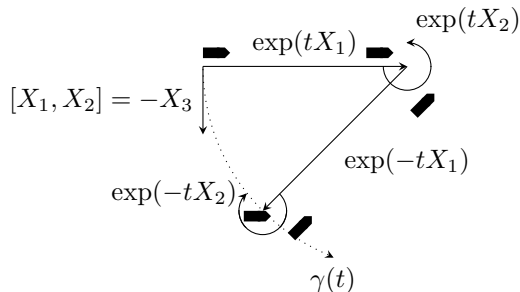


FIGURE 1. Modeling $SE(2)$ as a car with orientation, where X_1 is forward movement and X_2 is counter-clockwise rotation. Translation in the direction X_3 can be obtained by combining infinitesimal movements along X_1 and X_2 .

2.2. The visual cortex V1 and curve completion. When seeking to produce image processing algorithms, one option is to draw inspiration from the biological model that drives human perception. Visual information is processed in the brain by the *visual cortex*, located in the occipital lobe. *The primary visual cortex V1* is highly specialized in processing orientations and recognize patterns. From neurology we know that a neuron switches from its dormant state to its excited state when it gets sufficiently stimulated by either an external input or by other neurons [31].

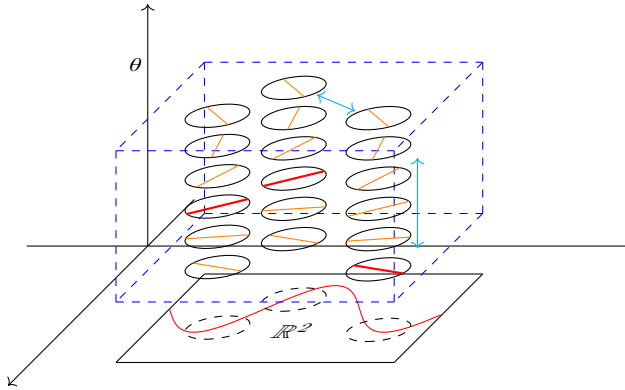


FIGURE 2. Visual Cortex V1 under a stimulus (red curve): the red orientation columns receive direct stimulus from the input, as opposed to the orange ones. Excitatory synapses for simple cells located in the same hypercolumn or that are spatially close and sensitive to the same orientation are indicated by cyan arrows.

Upon studying the visual cortex V1 one finds that the neurons are arranged in cells with elongated receptive fields, which exhibit even or odd symmetric patterns similar to Gabor filters [28]. In a simplified model, the neurons inside V1 are grouped into *orientation columns*, each being sensitive to stimuli at a specific point of the retina, corresponding to the spatial coordinate on the field of view, and a specific orientation. Orientation columns are themselves grouped together into *hypercolumns* that are sensitive to stimuli in a certain position of the retina, regardless of the orientation. Orientation columns are connected in two different ways: *vertical* (inhibitory) synapses and *horizontal* (excitatory) synapses. The vertical connections happen between columns belonging to the same hypercolumn, whereas horizontal ones happen between columns belonging to different hypercolumns that are spatially close and have similar orientation sensitivity. See Figure 2 for an illustration.

We can model V1 as $SE(2)$, where the hypercolumns are given as coordinates (x, y) and the orientation sensitivity of the orientation columns is given by θ . Because of the inhibitory synapses, we are only allowed to move along directions X_2 (within a hypercolumn) and X_1 (between hypercolumns).

We remark that the orientations mentioned are directionless, and so the correct space would be $PT\mathbb{R}^2 := SE(2)/\simeq$ which is the result of the identification $(x, y, \theta) \simeq (x, y, \theta + \pi)$. The notation reflects that $PT\mathbb{R}^2$ can be considered as the space of lines in the tangent space. See e.g. [8] for details. However, we can continue to develop our theory on $SE(2)$ as long as we are using operations that are invariant under the identification \simeq . This has the advantage that we can use global formulas for the vector fields X_1, X_2, X_3 , though we note that X_1^2, X_2^2 and X_3^2 are invariant under quotient by \simeq .

The human brain tries to “fill in” the gaps between curves or edges that present similar orientations while enhancing the contrast of objects that present different orientations. For a more mathematical description, let $\gamma_0 : [a, b] \cup [c, d] \rightarrow \mathbb{R}^2$, $a < b < c < d$, be a smooth curve, parametrized by arc length, that is partially hidden in the interval $t \in (b, c)$. We want to find a curve $\gamma : [b, c] \rightarrow \mathbb{R}^2$, parametrized by arc length that completes γ_0 while minimizing some cost $E[\gamma]$. We require that $\gamma(b) = \gamma_0(b)$, $\gamma(c) = \gamma_0(c)$ and for initial and final derivatives, $\dot{\gamma}(b) = \pm \dot{\gamma}_0(b)$ and $\dot{\gamma}(c) = \pm \dot{\gamma}_0(c)$. We are looking for a curve that is as smooth as possible, in the sense that the curve needs to minimize the energy $E_\beta(\gamma) = \int_b^c (1 + \beta |K_\gamma(s)|^2) ds$, $\beta > 0$, with the geodesic curvature given by $K_\gamma(t) = \frac{\dot{x}\ddot{y} - \dot{y}\ddot{x}}{(\dot{x}^2 + \dot{y}^2)^{\frac{3}{2}}}$.

Operationally we can find such curves by lifting the problem to $\text{SE}(2)$ and considering a curve $\Gamma(t) = (\gamma(t), \theta(t))$ in $\text{SE}(2)$ with $\dot{\gamma}(b) = \pm(\cos \theta(b)\partial_x + \sin \theta(b)\partial_y)$ and $\dot{\gamma}(c) = \pm(\cos \theta(c)\partial_x + \sin \theta(c)\partial_y)$. Curves minimizing the energy $E_\beta(\gamma)$ can then be considered as projections of sub-Riemannian geodesics in $\text{SE}(2)$. To give more details, let $\mathcal{H} = \text{span}\{X_1, X_2\} \subsetneq T\text{SE}(2)$ be as in Section 2.1. We introduce a smoothly varying inner product $g_\beta = \langle \cdot, \cdot \rangle_\beta$ defined just on \mathcal{H} by identities

$$\langle X_1, X_1 \rangle_\beta = 1, \quad \langle X_1, X_2 \rangle_\beta = 0, \quad \langle X_2, X_2 \rangle_\beta = \beta^{-1}.$$

This fiber metric g_β on \mathcal{H} is then called a *sub-Riemannian metric*, and the pair (\mathcal{H}, g_β) will be a *sub-Riemannian structure*. Geodesics of such a sub-Riemannian metric are then curves $\Gamma(t)$ that are tangent to \mathcal{H} and minimize the length with respect to g_β ,

$$\text{length}_\beta(\Gamma) = \int_b^c \|\dot{\Gamma}(t)\| dt = \int_b^c \sqrt{\langle X_1, \dot{\Gamma}(t) \rangle_\beta + \langle X_2, \dot{\Gamma}(t) \rangle_\beta} dt.$$

For more on sub-Riemannian geodesics, see Appendix A.1. We remark that the requirement that Γ is tangent to \mathcal{H} is exactly analogous to just moving in the “admissible directions of V1”, where a smaller β indicates an increased cost of moving within a hypercolumn. For a proof that the problem of minimizing the energy E_β is equivalent to the sub-Riemannian problem, see [8].

2.3. Curve completion in image processing. In the concrete applications described in this work, which are in the field of image processing, one will not find curves to complete and functionals to minimize, but rather corrupted images to restore. Images can be thought of in terms of curves if one takes into consideration the level curves of the image function, i.e. non-degenerate connected components of the level sets, as in this case, we need to treat multiple curves at once.

As described in [11, 34] one can approach this problem by considering in a stochastic way all possible admissible paths starting at the endpoint of the curve to reconstruct, and model the controls by independent Wiener processes u_t and v_t obtaining the following SDE:

$$\begin{pmatrix} dx_t \\ dy_t \\ d\theta_t \end{pmatrix} = \sqrt{2}X_1 \circ du_t + \sqrt{2\beta}X_2 \circ dv_t = \sqrt{2} \begin{pmatrix} \cos \theta_t \\ \sin \theta_t \\ 0 \end{pmatrix} \circ du_t + \sqrt{2\beta} \begin{pmatrix} 0 \\ 0 \\ 1 \end{pmatrix} \circ dv_t$$

The diffusion process associated to such SDE is $\frac{\partial \Psi}{\partial t} = \Delta_\beta \Psi$ where

$$\Delta_\beta = X_1^2 + \beta X_2^2 = \left(\cos \theta \frac{\partial}{\partial x} + \sin \theta \frac{\partial}{\partial y} \right)^2 + \beta \frac{\partial^2}{\partial \theta^2}.$$

We remark that Δ_β is symmetric with respect to the volume $d\mu = |dx \wedge dy \wedge d\theta|$ which is the Haar measure on $\text{SE}(2)$. We call Δ_β the *sub-Laplacian* of g_β . The operator Δ_β is not elliptic, but it has a smooth, strictly positive heat kernel $p_t(x, y)$ with respect to $d\mu$. For more on such operators, see Appendix A.2. In the next section, we will introduce a classic approach to image inpainting exploiting the fact that Δ_β is the intrinsic sub-Laplacian operator of $\text{SE}(2)$ endowed with sub-Riemannian structure (\mathcal{H}, g_β) .

3. SUB-RIEMANNIAN APPLICATION TO IMAGE PROCESSING

3.1. The classical inpainting algorithm. The inpainting algorithm proposed by Citti and Sarti [16] and improved by Boscaïn, Duplaix, Gauthier and Rossi [11], is a “blind algorithm”, i.e. it makes no assumption on the position of the corruption, and is therefore applied to the whole image without distinction between which areas contain noise and which areas do not. The input of the algorithm is a grayscale image, a signal from a rectangular portion $R \subset \mathbb{R}^2$ with values between 0 and 1, where 0 is regarded as white and 1 as black. This is in contrast with the usual convention in image processing and is due to the fact that the details on a photographic picture

are most commonly black rather than white. Corruption is represented as an area of constant value 0 (white). This can be changed in order to adapt to the nature of the corruption.

Let $\Pi : \text{SE}(2) \rightarrow \mathbb{R}^2$ be the projection. Recall that for a continuously differentiable image $I : \mathbb{R}^2 \supset R \rightarrow [0, 1]$ the derivative $X_3(I \circ \Pi)$ at (x, y, θ) takes the form

$$X_3(I \circ \Pi)(x, y, \theta) = -\sin(\theta)(\partial_x I)(x, y) + \cos(\theta)(\partial_y I)(x, y),$$

which gives the derivative of I in the direction of the vector $(-\sin \theta, \cos \theta)$. Let us for simplicity write $X_3(I \circ \Pi)$ simply as $X_3 I$. The maximum of $\theta \mapsto |X_3 I(x, y, \theta)|^2$ is achieved when $(-\sin \theta, \cos \theta)$ is parallel to the gradient $\nabla I(x, y)$. If the level curve of the image is defined at a point, it follows that such maximum is achieved when $(\cos \theta, \sin \theta)$ is the direction of the level curve at that point, regardless of orientation.

Recall that a smooth function $f : \mathbb{R}^2 \rightarrow \mathbb{R}$ is said to be Morse if it has only isolated critical points with nondegenerate Hessian. For such a function the points for which the direction of the level curve is not well defined are isolated. It is a known result that f defined to be $f := I * G_s$, the convolution with a Gaussian of standard deviation $s_x = s_y := s > 0$, is generically a Morse function [11]. From now on let I denote the convolution of the original image by a Gaussian of standard deviation $s > 0$ rather than the raw image itself.

Let $O : \text{SE}(2) \rightarrow [0, 1]$ be defined by

$$O(x, y, \theta) := \begin{cases} I(x, y) & \text{if } |X_3 I|(x, y, \theta) = \max_{\phi} |X_3 I|(x, y, \phi), \\ 0 & \text{otherwise,} \end{cases}$$

and mapping a non-critical point (x, y, θ) to the value of the image at (x, y) if θ is the direction of the level curve at the point (x, y) , regardless of orientation, or zero otherwise. The whole image domain is lifted in $\text{SE}(2)$ on the domain

$$\Sigma_0 = \{(x, y, \theta) : |X_3 I|(x, y, \theta) = \max_{\phi} |X_3 I|(x, y, \phi) > 0\}$$

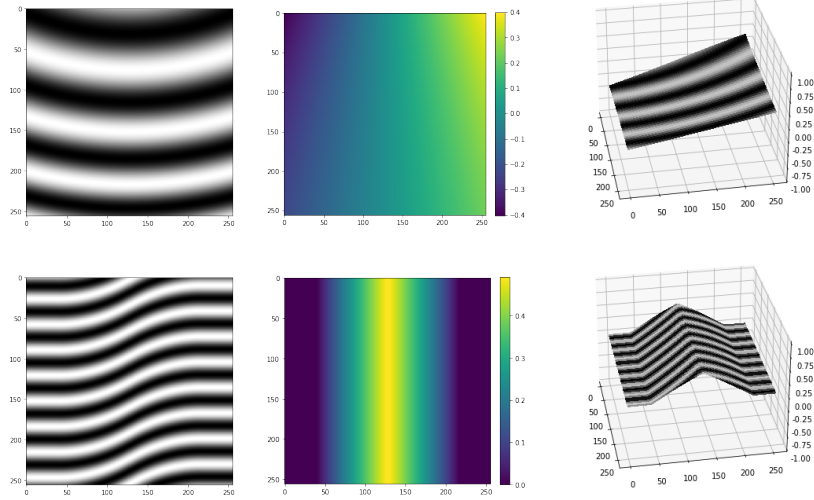


FIGURE 3. Examples of lifted images. In the first column are the original images, in the second column the orientation of the level lines, and in the third column, the images lifted to $\text{SE}(2)$, suppressing the trivial zero values for visualization purposes.

The lifted set corresponds to the maximum of activity of the output of simple cells that are stimulated exclusively by external signals, which can be modeled mathematically as a Dirac mass concentrated on Σ_0

$$(3.1) \quad \tilde{I}(x, y, \theta) = O(x, y, \theta)\delta_{\Sigma_0}.$$

$\tilde{I}(x, y, \theta)$ then corresponds to the image as perceived by our model of V1, where all the neural activity is concentrated on the Dirac mass δ_{Σ_0} . Integrating over a fiber $\Pi^{-1}(x, y) \cong S^1$ that is non-critical at position (x, y) yields exactly $I(x, y)$. If a point happens to be critical for the function $I(x, y)$, then by definition will not be part of Σ_0 since the gradient at that point vanishes.

The result of the restoration process is given by computing the solution $u(t, x, y, \theta)$ at time T of

$$(3.2) \quad \begin{cases} \partial_t u = \Delta_\beta u, \\ u(0, x, y, \theta) = \tilde{I}(x, y, \theta) \end{cases}$$

where $\Delta_\beta = X_1^2 + \beta X_2^2$. The parameter β is useful in practice to tune the “strength” of the diffusion that is performed in the direction X_2 compared to the direction X_1 . This corresponds to defining how strong are the horizontal and vertical excitatory synapses in the V1 biological model. The reconstructed image is recovered by projecting the solution $u(T, x, y, \theta)$ of the diffusion equation to \mathbb{R}^2 , either by integrating over fibers or by taking the maximum.

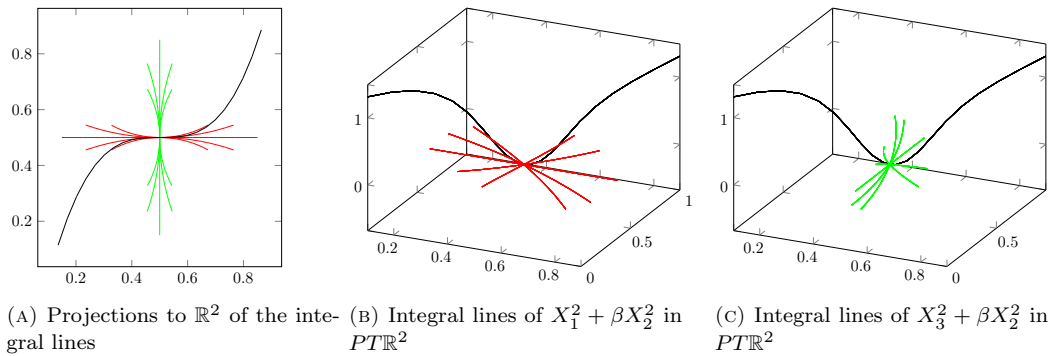


FIGURE 4. Integral lines of the vector fields $X_1^2 + \beta X_2^2$ (red) and $X_3^2 + \beta X_2^2$ (green) for a polynomial curve, at point $(\frac{1}{2}, \frac{1}{2})$, varying the coefficient β .

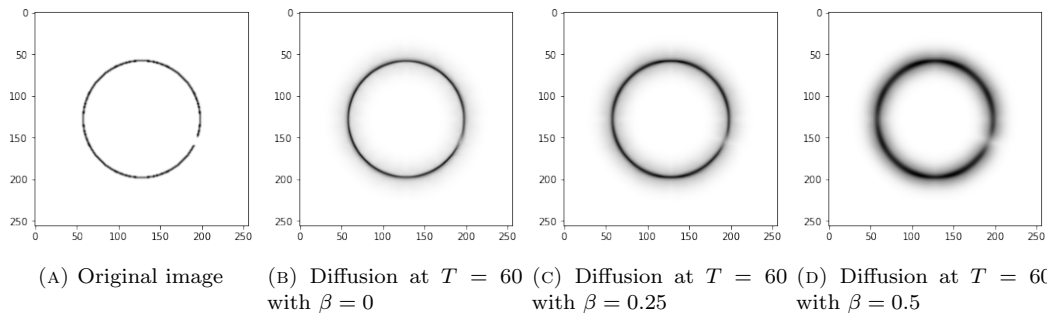


FIGURE 5. Application of the classic restoration algorithm to a basic example of a broken circle. We see that an increase in β produces a more spread-out diffusion.

Remark 3.1. One might get the impression from Figure 5, that we should keep β as small as possible or even zero. However, if we want to complete level curves where the endpoints do not have the same orientation, we will need some contributions X_2 for the level curves to rotate.

4. NEW INNOVATIONS IN THE SUB-RIEMANNIAN METHOD

4.1. Lift as a normal distribution. In the work by Marcelja [28] and Jones and Palmer [24] the similarity in behavior between simple cells and Gabor filters is studied and presented. For a Gabor filter with a fixed orientation θ the output of a signal through the filter decays exponentially as the angle of the original signal differs from θ . It is then argued that each hypercolumn behaves as a stack of Gabor filters with different orientations. From this idea of neural signal in the visual cortex V1 decaying exponentially as the angle in the fiber S^1 differs from the angle of the level curve, we can model each fiber as a normal distribution around the angle of the level curve. We are therefore “spreading” the input signal around the orientation of maximum response θ of the simple cells, and doing so following a Gaussian distribution centered around such orientation with this procedure

$$(4.1) \quad \tilde{I} = \mathcal{L}_\sigma(I) = (I \circ \Pi) \cdot \exp\left(-\frac{(X_1(I \circ \Pi))^2}{2\sigma^2|\nabla I|^2}\right) = (I \circ \Pi) \cdot \exp\left(-\frac{|\nabla I|^2 - (X_3(I \circ \Pi))^2}{2\sigma^2|\nabla I|^2}\right).$$

In other words, $I(x, y) \cdot \exp\left(-\left\langle \frac{\nabla I}{|\nabla I|}, (\cos \theta, \sin \theta) \right\rangle^2 / (2\sigma^2)\right)$, where we are using the σ^2 to adjust the variance around the optimal angle. The lift in (3.1) can be considered as a limiting case when $\sigma \rightarrow 0$.

Having defined such a lift $I \rightarrow \tilde{I}$, we need a projection process inverting this lift. The simplest projection that is inverse to \mathcal{L}_σ is the Π_{\max} is given by the maximum

$$\Pi_{\max}(\tilde{I})(x, y) = \max_{\theta} \tilde{I}(x, y, \theta).$$

However, we do not in general get a smooth function as a result of taking the maximum. An alternative projection can be defined as follows.

Theorem 4.1. *Define an operator $\Pi_\sigma : C^\infty(\text{SE}(2), (0, 1]) \rightarrow C^\infty(\mathbb{R}^2, (0, 1])$ by*

$$\Pi_\sigma(\tilde{I})(x, y) = \exp\left(\frac{1}{4\sigma} + \frac{1}{2\pi} \int_0^{2\pi} \ln \tilde{I}(x, y, \theta) d\theta\right).$$

Then $\Pi_\sigma(\mathcal{L}_\sigma(I)) = I$.

Proof. If $\tilde{I} = \mathcal{L}_\sigma(I)$, then averaging over a period yields

$$\int_0^{2\pi} \ln(\tilde{I}) d\theta = \int_0^{2\pi} \left(\ln I(x, y) - \frac{(\cos \theta \partial_x I + \sin \theta \partial_y I)^2}{2\sigma^2|\nabla I|^2} \right) d\theta = 2\pi \left(\ln I(x, y) - \frac{1}{4\sigma} \right)$$

We hence recover the original image I from this procedure. \square

The maximum Π_{\max} will in general be more computationally efficient, and our experiments show that problems of non-differentiability is not a large issue in practice. It also coincides with the projection used in earlier literature. It is however susceptible to fading under diffusion for small values of σ .

Let $u(t, x, y, \theta) = e^{t\Delta_\beta} \tilde{I}(x, y, \theta)$ be the solution of (3.2). Our main advantage by introducing the lifting \mathcal{L}_σ is that we prevent noise and fading of the image under the sub-Riemannian heat flow $e^{t\Delta_\beta}$.

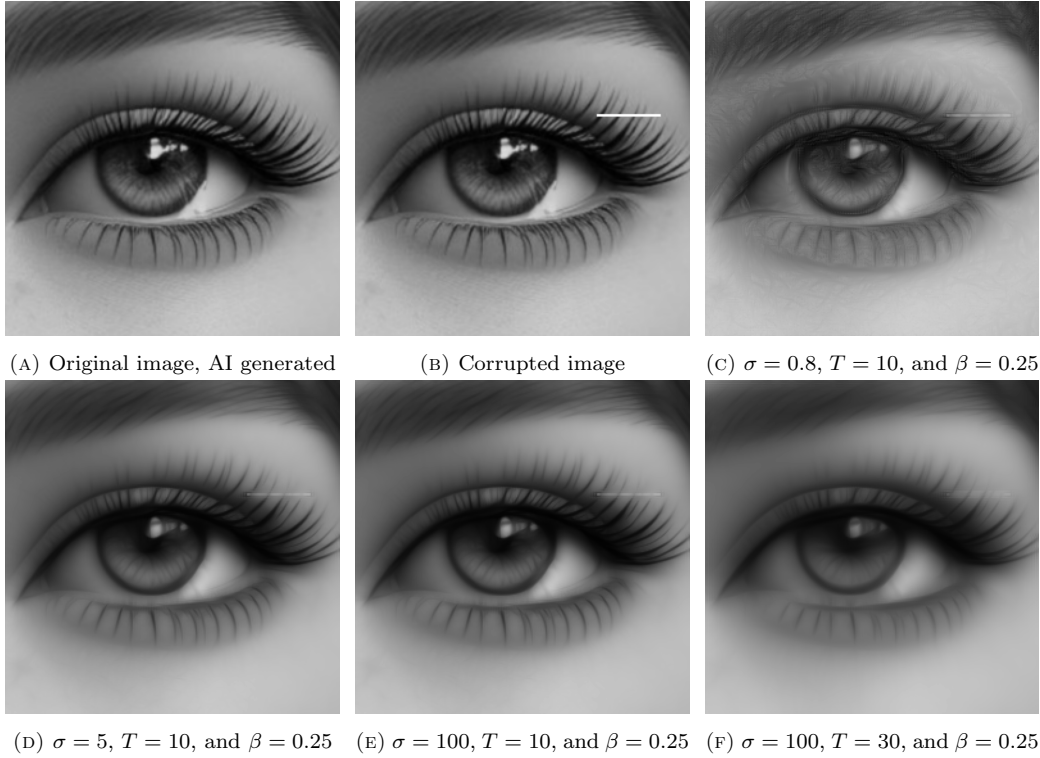


FIGURE 6. The original image (A) is lifted with Gaussian lift with different values for σ . We see that in (C), we quickly incur into fading and noise for small values of σ . This effect reduces for larger σ (D,E,F), even when considering a longer time scale (F).

We see that the resulting function after applying lift in $\mathcal{L}_\sigma(I)$ is π -periodic. It is hence sufficient to consider $\theta \in [0, \pi)$, which we can consider as working on $PT\mathbb{R}^2 = \text{SE}(2)/\simeq$. The projection Π_σ can then be defined using an average from 0 to π instead.

4.2. Preserving details through WaxOn, WaxOff. As we expect from a diffusion method, the result will not only inpaint along level curves but also blur the image. We can also see this from Figure 6 (D). In order to obtain sharper images after a diffusion, we will need to concentrate our image in the direction transverse to our level curves, that is, in the direction of X_3 . We therefore consider a second sub-Riemannian structure $\{\tilde{\mathcal{H}}, \tilde{g}_\beta\}$ on $\text{SE}(2)$, such that X_3 and $\frac{1}{\sqrt{\beta}}X_2$ forms an orthonormal basis. Let $\tilde{\Delta}_\beta$ be the operator

$$(4.2) \quad \tilde{\Delta}_\beta = X_3^2 + \beta X_2^2$$

Using the lift \mathcal{L}_σ as in (4.1), diffusion $e^{t\tilde{\Delta}_\beta}$ with $\tilde{\Delta}_\beta$ corresponds to diffusing transverse to level curves. The effect we are looking for is a reversing of this diffusion.

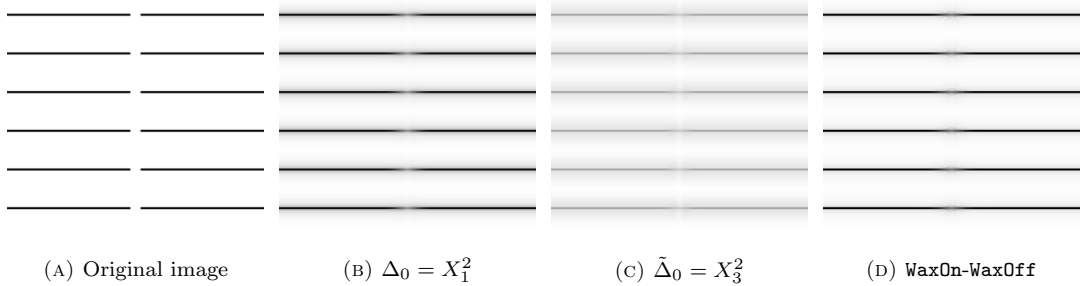


FIGURE 7. The original image (A) is lifted with Gaussian lift. Diffusion along X_1 is applied to obtain (B), while diffusion along X_3 yields (C). The **WaxOn-WaxOff** algorithm is used to obtain (D), which succeeds in connecting the lines while maintaining the overall image sharp

From this argument, we propose a new algorithm for image restoration: assuming that for small T we can recover the initial profile of neural activity by reversing the $\tilde{\Delta}_\beta$ -diffusion PDE, we can sharpen the restored image. Thus we first “put the wax on”, diffusing the image alongside the level lines, and then “get the wax off”, sharpening the image along X_3 . By alternating between applying **WaxOn**, that is $e^{t\Delta_\beta}$ for completion of level lines, then applying **WaxOff**, that is $e^{-t\tilde{\Delta}_\beta}$, to concentrate the image on these lines.

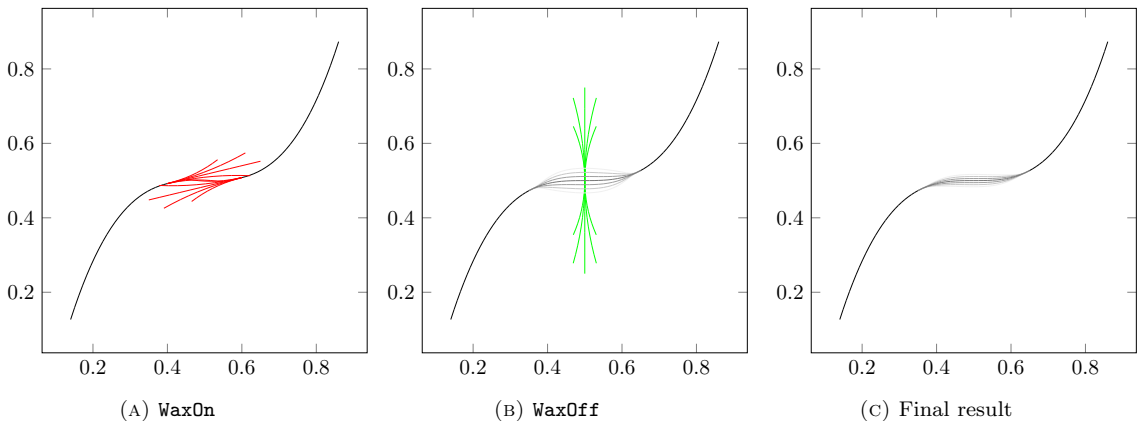


FIGURE 8. Sketch of intuition behind **WaxOn-WaxOff**

Although we are formally writing $e^{-t\tilde{\Delta}_\beta}$, the heat flow is an irreversible process and the solution of the heat equation for $t < 0$ is not well defined ([18], [36]). This is an ill-posed problem as we in general do not have stability with respect to initial data. See e.g. [40] and [25, Chapter 8.2] for details. Reversing the effect of the heat flow is susceptible to noise and will eventually diverge “blowing up”. In practice, the **WaxOff** needs to be run only up to a small time T_2 before any blowup happens.

By applying the two steps repeatedly, the **WaxOn** portion of the algorithm yields restoration while the **WaxOff** portion sharpens the result while retaining restored information.

Our rule of thumb from experiments is that running **WaxOn** for a time T , followed by applying **WaxOff** up until a time $T_2 = T/8$ yields empirically good results. The result is more stable for larger β , say $\beta = 2$, compared to smaller β -values.

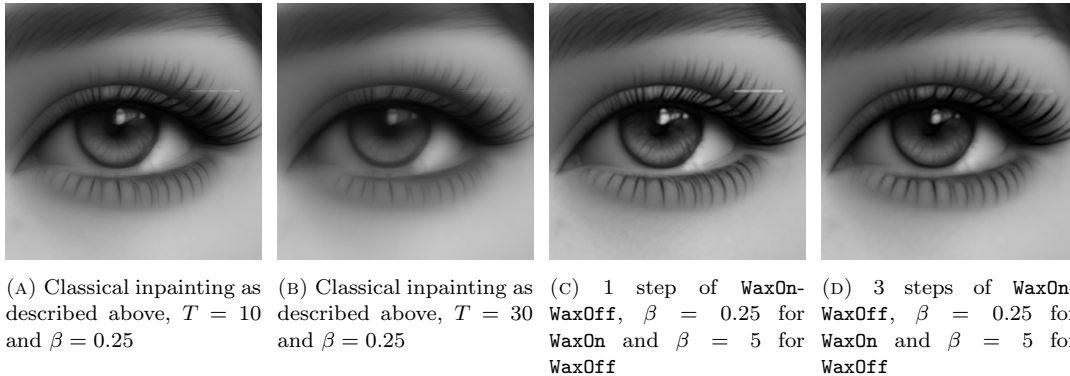


FIGURE 9. The usual algorithm (our implementation) is applied to obtain (A) and (B). One iteration of WaxOn-WaxOff for small T_2 produces (C) while multiple iterations of WaxOn-WaxOff are sequentially applied to produce (D) which achieves a similar level of restoration to (B) but maintains an overall sharper image.

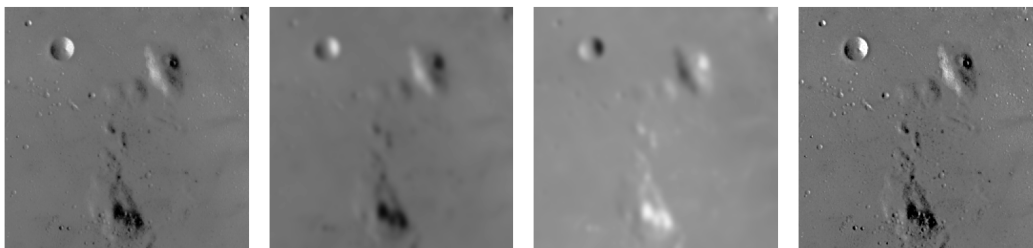
Remark 4.2. There are several suggested methods for stabilizing solutions for the inverse heat conduction, which might increase the time we could apply WaxOff. We refer to [2, 3, 4, 27, 39, 40] as examples of such methods.

4.3. Unsharp masking. The need to recover sharp images from blurred ones has been of interest in photography long before the invention of digital computers. In a photographic darkroom, this result can be physically achieved by copying the original glass-plate negative of the image, blurring it intentionally, and producing a scaled negative of it. If the two glass plates are now stacked one in front of the other and light is passed through both, the resulting image will see low-frequency information reduced while high-frequency information (acutance) enhanced.

In digital image processing, where glass-plate images are now arrays (matrices) and blurring is convolution with a normal distribution G of mean $\mu = 0$ and standard deviation s , such technique takes the form

$$I \mapsto I + C(I - I * G_s)$$

where I is the digital image, G_s is the normal distribution, and $C \in \mathbb{R}$ is the sharpening factor [20].



(A) Original image, courtesy of [38]

(B) Gaussian blur with $\sigma = 5$ is applied

(C) Negative of the blurred image

(D) Sharpened image with $C = 1$

FIGURE 10. Example of usage of the unsharp filter applied to a low-contrast image of the surface of the moon

If we consider kernels of size 3, this takes the form of a convolution with matrices of the form

$$\begin{bmatrix} 0 & 0 & 0 \\ 0 & 1 & 0 \\ 0 & 0 & 0 \end{bmatrix} + C \left(\begin{bmatrix} 0 & 0 & 0 \\ 0 & 1 & 0 \\ 0 & 0 & 0 \end{bmatrix} - \frac{1}{C} \begin{bmatrix} 0 & 1 & 0 \\ 1 & 1 & 1 \\ 0 & 1 & 0 \end{bmatrix} \right) = \begin{bmatrix} 0 & -1 & 0 \\ -1 & C & -1 \\ 0 & -1 & 0 \end{bmatrix}$$

The case $C = 5$ is the usual unsharp filter of dimension 3, commonly used in image processing applications.

It comes quite naturally to consider an extension of unsharp masking to other domains, such as $SE(2)$, to produce a curvature-sensitive sharpening filter aimed at enhancing digital images according to the mechanisms of the visual cortex V1.

The effect of the undesired blurring is therefore the solution at time T to the Cauchy problem

$$\tilde{\Delta}_\beta = X_3^2 + \beta X_2^2 \quad \begin{cases} \partial_t u = \tilde{\Delta}_\beta u, \\ u(0, x, y, \theta) = \tilde{I}(x, y, \theta) \end{cases}$$

Denote such solution by $\tilde{I}_T(x, y, \theta) = u(T, x, y, \theta)$. Then the unsharp masking in $SE(2)$ takes the form $\tilde{I} + C(\tilde{I} - \tilde{I}_T)$ for a sharpening factor C .

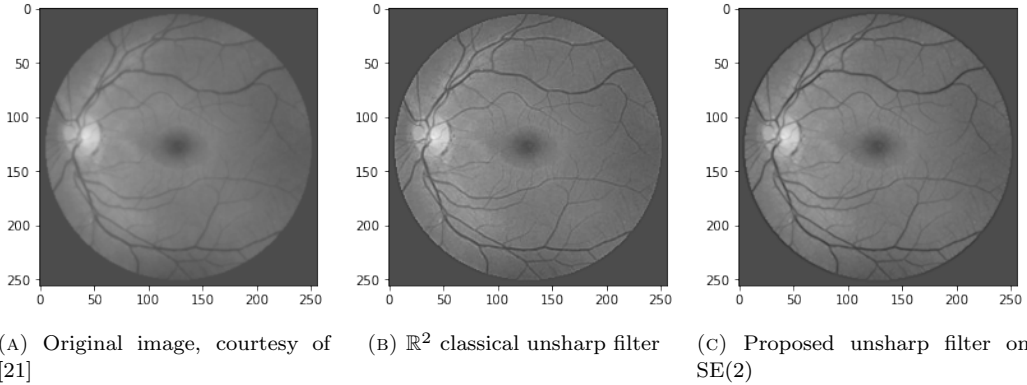


FIGURE 11. Retinal image (A) sharpened using the classical unsharp filter over \mathbb{R}^2 (B) and using the proposed sharpening method, after projection (C).

Defining an extension of the unsharp filter over $SE(2)$ rather than \mathbb{R}^2 allows us to work with a lifted image in its natural domain rather than alternating projections and lifts. Combining the orientation-sensitive diffusion equation with unsharp filtering provides an effective tool to enhance the contrast of particularly predisposed images such as retinal scans, or used as a preprocessing step in a more complex pipeline.

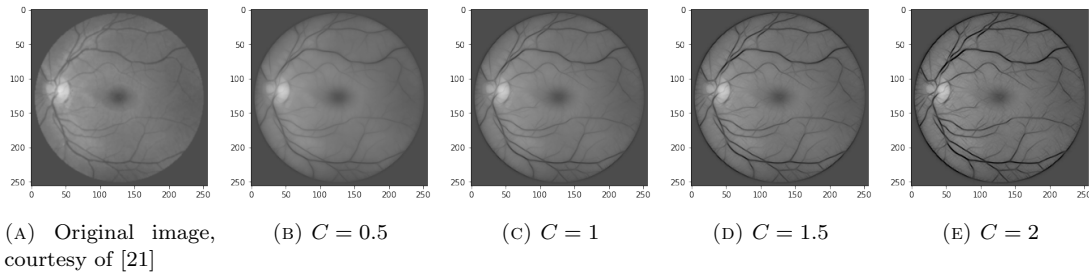


FIGURE 12. The original image (A) is processed with diffusion under $\Delta_\beta = X_1^2 + \beta^2 X_2^2$ and sharpened with varying coefficient C (B,C,D,E)

4.4. WaxOn-WaxOff in the AHE algorithm. Boscain, Chertoviskih, Gauthier, Prandi, and Remizov have introduced the AHE algorithm [13] as a strikingly powerful algorithm for image restoration when dealing with a variation of the problem in which the position of the corruption is known. We propose an enriched version of this algorithm which produces a sharper final result with higher contrast.

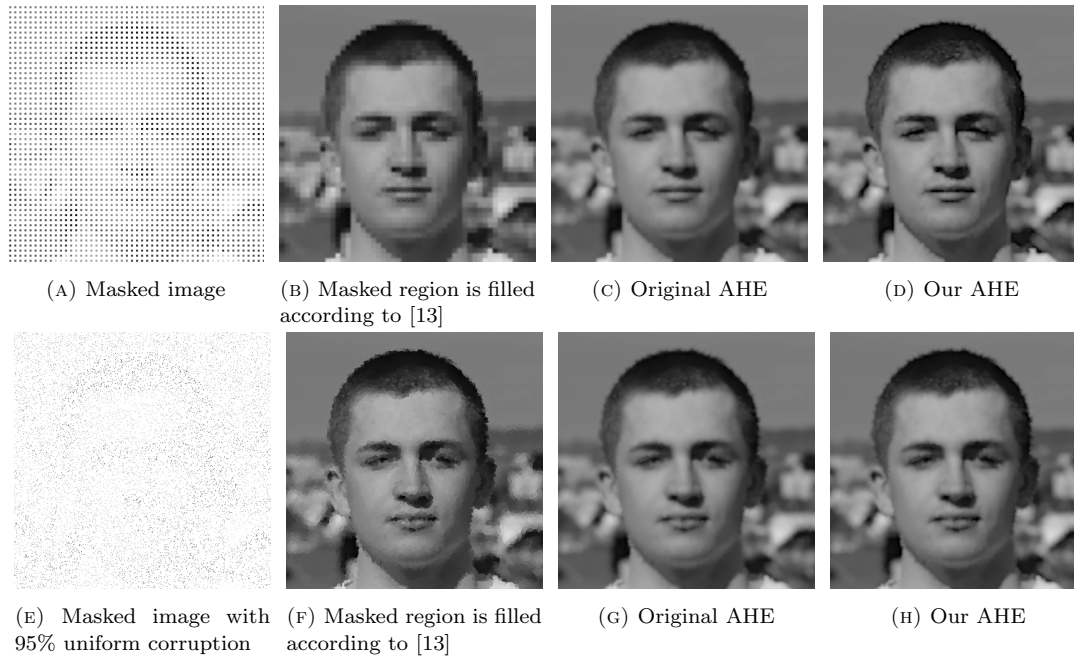


FIGURE 13. Example of image restoration with a known mask using AHE algorithm enriched by Gaussian lift and **WaxOn-WaxOff**. The last column shows a result with a higher contrast, due to the unsharp filter applied in the procedure.

In our implementation, the images are lifted via Gaussian lift and subsequently, the **WaxOn-WaxOff** procedure is applied, with $SE(2)$ -unsharp used as **WaxOff**, together with advanced averaging as introduced in [13]. These two operations are performed repeatedly removing at each step the contour of the corrupted portion from the mask according to 4-point connectivity. The procedure is run until the mask is exhausted. In this way the images after smoothing become

progressively sharper, as the mask is reduced step by step and advanced average is performed on a progressively decreasing number of pixels.

APPENDIX A. GEOMETRIC PRELIMINARIES

A.1. Sub-Riemannian manifolds. To introduce the reader who is unfamiliar with sub-Riemannian geometry we give here an introduction of the main concepts and results from the field. For a more in-depth study on the subject, we redirect to [30].

Definition A.1. *A sub-Riemannian manifold is a triplet (M, \mathcal{H}, g) with M being a connected manifold, $\mathcal{H} \subset TM$ a linear subbundle and $g = \langle \cdot, \cdot \rangle$ a fiber-metric defined on the subbundle \mathcal{H} .*

We call $\mathcal{H} \subset TM$ in this definition the *horizontal distribution*. A sub-Riemannian manifold can be considered as a limiting case of a Riemannian manifold where the distances of vectors outside of \mathcal{H} approach infinity. Curves $\gamma : [a, b] \rightarrow M$ with a finite length will then need to be a *horizontal curve*: an absolutely continuous curve satisfying $\dot{\gamma}(t) \in \mathcal{H}_{\gamma(t)}$ for almost every t . For such a curve, we can define its length by

$$\text{length}(\gamma) = \int_a^b \langle \dot{\gamma}(t), \dot{\gamma}(t) \rangle^{1/2} dt.$$

We can then also introduce the corresponding sub-Riemannian distance by

$$d_g(x, y) = \inf \left\{ \text{length}(\gamma) \mid \begin{array}{l} \gamma : [a, b] \rightarrow M \text{ horizontal} \\ \gamma(a) = x, \gamma(b) = y \end{array} \right\}.$$

In general, there might not be any curve connecting a point x and y , meaning that the distance above will be infinite. It is therefore typical to require the horizontal bundle \mathcal{H} to be bracket-generating. Let $\mathfrak{X}_{\mathcal{H}}$ be all vector fields taking values in the subbundle \mathcal{H} . We then define $\hat{\mathfrak{X}}_{\mathcal{H}} \supseteq \mathfrak{X}_{\mathcal{H}}$ as the space of all vector fields generated by those in $\mathfrak{X}_{\mathcal{H}}$ and their iterated Lie brackets. In other words

$$\hat{\mathfrak{X}}_{\mathcal{H}} = \text{span} \left\{ [X_{i_1}, [X_{i_2}, [\dots [X_{i_{l-1}}, X_{i_l}] \dots]] \mid X_{i_j} \in \mathfrak{X}_{\mathcal{H}}, l = 1, 2, 3, \dots \right\},$$

where we interpret the case $l = 1$ simply as the vector field X_{i_1} itself.

Definition A.2. *We say that \mathcal{H} is bracket-generating if for every $x \in M$,*

$$T_x M = \{X(x) : X \in \hat{\mathfrak{X}}_{\mathcal{H}}\}.$$

In other words, \mathcal{H} is bracket generating if we can make a partial derivative in any direction we want by combining directions in \mathcal{H} . By the Chow-Rashevskii theorem [14, 35], any two points in a sub-Riemannian manifold can be connected by a horizontal curve if \mathcal{H} is bracket-generating. Furthermore, d_g will be a well-defined metric distance that has the same open sets as on the original manifold.

For horizontal curves connecting a point and x and y in M , this curve γ can either be *regular* or *singular*, depending on whether or not the space of horizontal curves from x to y have the structure of a Banach manifold close to γ . See [29] for the formal definition and how to deal with the case when such curves are minimizers. Length minimizers that are regular will be *normal sub-Riemannian geodesics*; projections of solutions of the Hamiltonian system corresponding to the sub-Riemannian Hamiltonian. This Hamiltonian is locally given as

$$H(p) = \frac{1}{2} \sum_{i=1}^k p(X_i)^2, \quad p \in T^*M,$$

where X_1, \dots, X_k is a local orthonormal basis of \mathcal{H} . We remark the following condition, see e.g. [1, Section 20.5.1], which holds for our case of Section 2.1.

Theorem A.3 (Goh condition). *If \mathcal{H} satisfies for any $x \in M$,*

$$T_x M = \text{span}\{X_0(x), [X_1, X_2](x) \mid X_0, X_1, X_2 \in \mathfrak{X}_{\mathcal{H}}\},$$

then all length minimizers will be normal minimizers.

A.2. Sub-Laplacians and hypoellipticity. Consider a second order operator L on a manifold M , which in local coordinates can be written as

$$L = \sum_{i,j=1}^n a_{ij}(x) \frac{\partial^2}{\partial x_i \partial x_j} + \sum_{j=1}^n b_j(x) \frac{\partial}{\partial x_j},$$

with $(a_{ij}(x))$ being positive semi-definite with a constant rank k . Such an operator can then locally be written as $L = \sum_{k=1}^k X_k^2 + X_0$. We can then define a sub-Riemannian structure on (\mathcal{H}, g) on M by making X_1, \dots, X_k into a local orthonormal basis. There are several such operators corresponding to the same sub-Riemannian structure, but given a volume density, only one will be *symmetric* with respect to a given volume density $d\mu$. By symmetric, we mean that $\int_M f_1(Lf_2)d\mu = \int_M f_2(Lf_1)d\mu$ for any pair of smooth functions $f_1, f_2 \in C_0^\infty(M)$ of compact support, and we remark that requiring L to be symmetric means that we locally have

$$L = \sum_{j=1}^k (X_j^2 + (\text{div}_{d\mu} X_j)X_j).$$

We call this operator *the sub-Laplacian of (M, \mathcal{H}, g) and $d\mu$* . We now have the following result, by combining results of [23], [37], and [26].

Theorem A.4. *Let L be the sub-Laplacian of a sub-Riemannian structure (M, \mathcal{H}, g) with volume element $d\mu$. Assume that \mathcal{H} is bracket-generating. Then L and the heat operator $\partial_t - L$ are hypoelliptic. Furthermore, for the heat-semigroup e^{tL} , we have density*

$$e^{tL} f(x) = \int_M p_t(x, y) f(y) d\mu,$$

where $p_t(x, y)$ is a smooth, strictly positive function that is symmetric in x and y . Furthermore, we have short-time asymptotics

$$\lim_{t \downarrow 0} 2t \log p_t(x, y) = -d_g(x, y)^2.$$

REFERENCES

- [1] A. A. Agrachev and Y. L. Sachkov. *Control theory from the geometric viewpoint*, volume 87 of *Encyclopaedia of Mathematical Sciences*. Springer-Verlag, Berlin, 2004. Control Theory and Optimization, II.
- [2] O. M. Alifanov, E. Artioukhine, and S. Romyantsev. *Extreme methods for solving ill-posed problems with applications to inverse heat transfer problems*. Begell house, 1995.
- [3] J. V. Beck. Nonlinear estimation applied to the nonlinear inverse heat conduction problem. *International Journal of heat and mass transfer*, 13(4):703–716, 1970.
- [4] J. V. Beck, B. Blackwell, and A. Haji-Sheikh. Comparison of some inverse heat conduction methods using experimental data. *International Journal of Heat and Mass Transfer*, 39(17):3649–3657, 1996.
- [5] E. Bekkers, R. Duits, T. Berendschot, and B. ter Haar Romeny. A Multi-Orientation Analysis Approach to Retinal Vessel Tracking. *J. Math. Imaging Vision*, 49(3):583–610, July 2014.
- [6] E. J. Bekkers, M. W. Lafarge, M. Veta, K. A. J. Eppenhof, J. P. W. Pluim, and R. Duits. Roto-Translation Covariant Convolutional Networks for Medical Image Analysis. *arXiv*, Apr. 2018.
- [7] U. Boscain, G. Charlot, and F. Rossi. Existence of planar curves minimizing length and curvature. *Proceedings of the Steklov Institute of Mathematics*, 270, 06 2009.
- [8] U. Boscain, G. Charlot, and F. Rossi. Existence of planar curves minimizing length and curvature. *Proc. Steklov Inst. Math.*, 270(1):43–56, Sept. 2010.
- [9] U. Boscain, R. Chertovskih, J.-P. Gauthier, D. Prandi, and A. Remizov. Cortical-inspired image reconstruction via sub-riemannian geometry and hypoelliptic diffusion. *ESAIM Proc. Surv.*, 64:37–53, 2018.

- [10] U. Boscain, R. A. Chertovskih, J. P. Gauthier, and A. O. Remizov. Hypocoelliptic diffusion and human vision: A semidiscrete new twist. *SIAM J. Imaging Sci.*, 7(2):669–695, jan 2014.
- [11] U. Boscain, J. Duplaix, J.-P. Gauthier, and F. Rossi. Anthropomorphic image reconstruction via hypocoelliptic diffusion. *SIAM j. control optim.*, 50(3):1309–1336, jan 2012.
- [12] U. Boscain and M. Sigalotti. Introduction to controllability of nonlinear systems. In *Contemporary Research in Elliptic PDEs and Related Topics*, pages 203–219. Springer, 2019.
- [13] U. V. Boscain, R. Chertovskih, J.-P. Gauthier, D. Prandi, and A. Remizov. Highly corrupted image inpainting through hypocoelliptic diffusion. *J. Math. Imaging Vis.*, 60(8):1231–1245, oct 2018.
- [14] W.-L. Chow. Über Systeme von linearen partiellen Differentialgleichungen erster Ordnung. *Math. Ann.*, 117:98–105, 1939.
- [15] G. Citti, B. Franceschiello, G. Sanguinetti, and A. Sarti. Sub-Riemannian mean curvature flow for image processing. *SIAM J. Imaging Sci.*, 9(1):212–237, jan 2016.
- [16] G. Citti and A. Sarti. A cortical based model of perceptual completion in the roto-translation space. *J. Math. Imaging Vis.*, 24(3):307–326, may 2006.
- [17] R. DUTS and E. FRANKEN. Left-invariant parabolic evolutions on $se(2)$ and contour enhancement via invertible orientation scores part i: Linear left-invariant diffusion equations on $se(2)$. *Quarterly of Applied Mathematics*, 68(2):255–292, 2010.
- [18] L. C. Evans. *Partial Differential Equations*. American Mathematical Society, 2010.
- [19] E. Franken and R. Duits. Crossing-Preserving Coherence-Enhancing Diffusion on Invertible Orientation Scores. *Int. J. Comput. Vision*, 2009.
- [20] R. C. Gonzalez and R. E. Woods. *Digital Image Processing*. Prentice Hall, Upper Saddle River, NJ, USA, 2008.
- [21] M. Häggström. Medical gallery of mikael häggström 2014. *WikiJournal of Medicine*, 1(2), 2014.
- [22] J. Hannink, R. Duits, and E. Bekkers. Crossing-Preserving Multi-scale Vesselness. In *Medical Image Computing and Computer-Assisted Intervention – MICCAI 2014*, pages 603–610. Springer, Cham, Switzerland, 2014.
- [23] L. Hörmander. Hypocoelliptic second order differential equations. *Acta Math.*, 119:147–171, 1967.
- [24] J. P. Jones and L. A. Palmer. An evaluation of the two-dimensional Gabor filter model of simple receptive fields in cat striate cortex. *J. Neurophysiol.*, Dec. 1987.
- [25] S. I. Kabanikhin. Inverse and ill-posed problems. In *Inverse and Ill-posed Problems*. de Gruyter, 2011.
- [26] R. Léandre. Minoration en temps petit de la densité d’une diffusion dégénérée. *J. Funct. Anal.*, 74(2):399–414, 1987.
- [27] J. Liu. A stability analysis on beck’s procedure for inverse heat conduction problems. *Journal of Computational Physics*, 123(1):65–73, 1996.
- [28] S. Marčelja. Mathematical description of the responses of simple cortical cells*. *JOSA*, 70(11):1297–1300, Nov. 1980.
- [29] R. Montgomery. *A tour of subriemannian geometries, their geodesics and applications*, volume 91 of *Mathematical Surveys and Monographs*. American Mathematical Society, Providence, RI, 2002.
- [30] R. Montgomery. *A Tour of Subriemannian Geometries, Their Geodesics and Applications*. American Mathematical Society, 2006. [Online; accessed 14. Jul. 2023].
- [31] A. Orhan E. *Neuroanatomical Basis of Clinical Neurology*. CRC Press, Boca Raton, FL, USA, Dec. 1969.
- [32] J. Petitot. *Neurogéométrie de la vision: modèles mathématiques et physiques des architectures fonctionnelles*. Les Éditions de l’École Polytechnique, 2008.
- [33] J. Petitot and Y. Tondut. Vers une neurogéométrie. Fibrations corticales, structures de contact et contours subjectifs modaux. *Mathématiques et sciences humaines. Mathematics and social sciences*, 145, Mar. 1999.
- [34] D. Prandi and J.-P. Gauthier. *A semidiscrete version of the Citti-Petitot-Sarti model as a plausible model for anthropomorphic image reconstruction and pattern recognition*. Springer, 2018.
- [35] P. K. Rashevskii. On the connectability of two arbitrary points of a totally nonholonomic space by an admissible curve. *Uchen. Zap. Mosk. Ped. Inst. Ser. Fiz.-Mat. Nauk*, 3(2):83–94, 1938.
- [36] W. A. Strauss. *Partial Differential Equations: An Introduction*. Wiley, Chichester, England, UK, 2007.
- [37] D. W. Stroock and S. R. S. Varadhan. On the support of diffusion processes with applications to the strong maximum principle. In *Proceedings of the Sixth Berkeley Symposium on Mathematical Statistics and Probability (Univ. California, Berkeley, Calif., 1970/1971)*, Vol. III: Probability theory, pages 333–359. Univ. California Press, Berkeley, Calif., 1972.
- [38] S. van der Walt, J. L. Schönberger, J. Nunez-Iglesias, F. Boulogne, J. D. Warner, N. Yager, E. Gouillart, and T. Yu. scikit-image: image processing in python. *PeerJ*, 2:e453, June 2014.
- [39] Y. Wang, J. Cheng, J. Nakagawa, and M. Yamamoto. A numerical method for solving the inverse heat conduction problem without initial value. *Inverse Problems in Science and Engineering*, 18(5):655–671, 2010.

- [40] C. F. Weber. Analysis and solution of the ill-posed inverse heat conduction problem. *International Journal of Heat and Mass Transfer*, 24(11):1783–1792, 1981.
- [41] J. Zhang, B. Dashtbozorg, E. Bekkers, J. P. W. Pluim, R. Duits, and B. M. ter Haar Romeny. Robust Retinal Vessel Segmentation via Locally Adaptive Derivative Frames in Orientation Scores. *IEEE Trans. Med. Imaging*, 35(12):2631–2644, Aug. 2016.